TABLE 2 Effect of mating on egg production rate

| Treatment | Eggs laid per hour Day 1 | Day 2 | Day 3 |
|---|---|---|---|
| Unmated | 6.1 ± 0.2 | 6.5 ± 1.5 | 0.6 ± 0.3 |
| Mated once | 5.0 ± 0.2 | 6.9 ± 0.2 | 5.4 ± 1.9 |
| Mated thrice | 4.9 ± 0.4 | 6.5 ± 0.1 | 5.1 ± 1.3 |

N2 hermaphrodites were mated singly with 10 N2 males for five hours (20 °C). The first group was unmated, the second mated only on day one, and the third on three consecutive days. Egg laying was measured over a three-hour period at 24-hour intervals, immediately after mating in the mating test groups. Each group consisted of six animals and the entire experiment was repeated twice. Rates are ±s.e. Non-parametric ANOVA (Kruskal-Wallis) revealed a nearly significant decrease in the rate of egg laying in the two mated groups on day 1 ($P = 0.07$), but not day 2. No increase in egg-laying rate was observed. On day 3, the self sperm of unmated animals were almost depleted.

males, which cannot mate owing to motility defects[21], were used. Maintenance in the presence of such males throughout life, at a male-to-hermaphrodite ratio of 2:1, did not reduce hermaphrodite longevity (data not shown).

These results demonstrate that the cost of mating to hermaphrodite longevity is not associated with egg production or egg laying, the receipt or storage of sperm, internal hatching of eggs, or non-mating effects associated with presence of males. Thus, it would appear that the stress of copulation reduces hermaphrodite lifespan, either directly or by increasing susceptibility to infection by the bacteria used as food. It also remains possible that receipt of seminal fluid is a cause. By contrast with the hermaphrodites, there is no apparent cost to males of increased spermatogenesis or copulation. Sterile hermaphrodites do not have increase lifespan[9–11] and mutations in only one of many genes involved in spermatogenesis, *spe-26*, have been reported to increase lifespan[12], suggesting that lifespan extension in *spe-26* mutants may be a pleiotropic effect unconnected to the defect in spermatogenesis. Taken together, these results do not support the hypothesis that increased gamete production accelerates ageing because of a drain on resources from somatic maintenance functions, or that mating actively stimulates such a diversion of resources. It is possible, however, that such trade-offs might only be observed when resources are limited, that is, in calorically restricted animals. □

Received 30 October; accepted 4 December 1995.

1. Williams, G. C. *Evolution* **11,** 398–411 (1957).
2. Kirkwood, T. B. L. *Nature* **270,** 301–304 (1977).
3. Partridge, L. & Harvey, P. H. *Science* **241,** 1449–1455 (1988).
4. Partridge, L., Green, A. & Fowler, K. *J. Insect Physiol.* **33,** 745–749 (1987).
5. Chapman, T., Liddle, L. F., Kalb, J. M., Wolfner, M. F. & Partridge, L. *Nature* **373,** 241–244 (1995).
6. Chapman, T. *J. Insect Physiol.* **38,** 223–227 (1992).
7. Partridge, L. & Farquhar, M. *Nature* **294,** 580–582 (1981).
8. Kimble, J. & Ward, S. in *The Nematode* Caenorhabditis elegans (ed. Wood, W. B.) 191–213 (Cold Spring Harbor Laboratory Press, New York, 1988).
9. Klass, M. R. *Mechanisms of Ageing and Development* **6,** 413–429 (1977).
10. Friedman, D. B. & Johnson, T. E. *Genetics* **118,** 75–86 (1988).
11. Kenyon, C., Chang, J., Gensch, E., Rudner, A. & Tabtiang, R. *Nature* **366,** 461–464 (1993).
12. Van Voorhies, W. A. *Nature* **360,** 456–458 (1992).
13. Argon, Y. & Ward, S. *Genetics* **96,** 413–432 (1980).
14. Ward, S. & Miwa, J. *Genetics* **88,** 285–303 (1978).
15. Ward, S., Argon, Y. & Nelson, G. A. *J. Cell Biol.* **91,** 26–44 (1981).
16. Kalb, J. M., DiBenedetto, A. J. & Wolfner, M. F. *Proc. natn. Acad. Sci. U.S.A.* **90,** 8093–8097 (1993).
17. Chen, P. S. *et al. Cell* **54,** 291–298 (1988).
18. Scott, D. *Anim. Behav.* **35,** 142–149 (1987).
19. Harshman, L. G. & Prout, T. *Evolution* **48,** 758–766 (1994).
20. Schedl, T. & Kimble, J. *Genetics* **119,** 43–61 (1988).
21. Hodgkin, J. *Genetics* **103,** 43–64 (1983).
22. Wilkinson, L. *SYSTAT: The System for Statistics* (Systat Inc., Evanston, Illinois, 1989).
23. Brenner, S. *Genetics* **77,** 71–94 (1974).
24. L'Hernault, S. W., Shakes, D. C. & Ward, S. *Genetics* **120,** 435–452 (1988).

ACKNOWLEDGEMENTS. We thank T. P. Holtsford for statistical analysis, W. Van Voorhies for the variant of the N2 strain, S. L'Hernault, P. S. Albert and C. V. Gunther for discussion, and J. Kimble for a *fog-2(q71)* strain. This research was funded by a University of Missouri Molecular Biology Fellowship to D.G. and a DHHS grant to D.L.R. Some nematode strains used in this study were provided by the *Caenorhabditis* Genetics Center.

# A systematic map of direction preference in primary visual cortex

**Michael Weliky, William H. Bosking & David Fitzpatrick**

Department of Neurobiology, Duke University Medical Center, Box 3209, Durham, North Carolina 27710, USA

**NEURONS in the primary visual cortex respond selectively to the orientation of edges and their direction of motion. Orientation preference is mapped in a systematic fashion across the cortical surface, such that neurons in adjacent columns have similar but slightly shifted preferred orientations[1–7]. Microelectrode studies have suggested that direction preference is also arranged in a systematic fashion[8–10], but exactly how this response property is mapped remains unclear. Here we show by optical imaging[4–5] of intrinsic signals[6–7,11–14] in ferret cortical area 17 that there is a mosaic-like map of direction preference. This map consists of numerous regions within which direction preference changes in a slow, continuous fashion. These regions are separated by winding boundaries (fractures) across which direction preference shifts abruptly, often by 180 °. Comparison of direction and orientation preference maps shows that these fractures subdivide iso-orientation domains into regions selective for opposite directions of motion.**

Functional maps of direction preference were obtained by collecting separate images of the cortical surface while the animal viewed bar stimuli moving in one of eight directions ($n = 13$ animals). Figure 1*a* shows differential images of direction preference obtained by subtracting the cortical images that were collected while the animal viewed stimuli that moved in opposite directions. These difference images are composed of numerous oval or circular-shaped dark and light patches (iso-direction domains). Iso-direction domains differ in their appearance from iso-orientation domains, which have a more banded or striped appearance (Fig. 1*b*). Neurons located within the centre of iso-direction domains have highly selective directional responses that can be predicted from the optical images ($n = 4$ animals, 10 recordings) (Figs 1*b*, *c* and 2*a*).

The complete organization of direction preferences across a region of visual cortex was determined by vectorially summing the eight images shown in Fig. 1*a*. The result is shown in Fig. 2*a*, where preferred direction is colour coded and indicated by the direction of the arrows overlaid on the map; the length of the arrows represents the magnitude of direction selectivity. The map consists of numerous, distinct regions of high selectivity in which direction preference shifts in a slow, continuous fashion. Figure 2*b* shows that these regions are separated by narrow bands of low selectivity across which direction preference changes abruptly, often by 180 °. In this image, arrows indicating direction preference are overlaid on a magnitude map of direction selectivity where black indicates regions of low selectivity.

Direction and orientation preference maps are similar in some characteristics and strikingly different in others. Both maps are organized at a similar spatial scale (Fig. 3*a*, *d*). Using autocorrelation analysis, we calculated the average repeat distance in the orientation preference map to be 890 ± 29 μm and in the direction preference map to be 867 ± 18 μm ($n = 5$ animals). But the fragmented structure of the direction preference maps, which is especially apparent when the magnitude of the direction signal is plotted (Fig. 3*b*), is very different from that found for orientation preference maps (Fig. 3*e*). Regions of low selectivity in orientation maps are confined to small circular zones located at the centres of orientation pinwheels or, less commonly, short lines that connect adjacent pinwheel centres[5–7]. This difference is also apparent

when rate of change maps for direction and orientation preference are compared (Fig. 3*c*, *f*); regions of low selectivity in both maps correspond to the regions in which the mapped response property changes most rapidly. Thus orientation maps are dominated by points of rapid change whereas direction maps are dominated by lines of rapid change (fractures).

The fragmented structure of the direction preference map may be understood in terms of the need to represent all orientations and directions for every point in visual space. To satisfy this requirement, two opposite directions of motion must be represented for each stimulus orientation. Consistent with this interpretation, we found that single iso-orientation domains are subdivided into numerous patches selective for motion in opposite directions (Fig. 4*a*). This subdivision of iso-orientation regions is also apparent when vector maps of direction and orientation preference are overlaid (Fig. 4*b*) and when direction fractures are viewed in relation to iso-orientation contour lines (Fig. 4*c*).

Even though the direction preference map is more fractured than the orientation map, both maps display a high degree of continuity. Indeed, the number and arrangement of direction fractures appears to maximize continuity in the mapping of direction preference within the constraints imposed by the orderly map of orientation. This is best illustrated by examining the direction preference map in the region of an orientation pinwheel. An orientation pinwheel represents a complete and continuous cycle of orientation values (each orientation appearing only once[6,7]). Although a complete cycle of orientation values is covered in 180°, the complete cycle of direction values requires 360° (that is, for each orientation there are two possible directions). Thus, even if direction is mapped as continuously as possible around an orientation pinwheel, at most, only half a direction cycle can be represented, and there must be at least one discontinuity in the direction preference map where contiguous cortical regions have opposite direction preferences. That we find examples of orientation pinwheels with single direction discontinuities (Fig. 4*d*) indicates that continuity is an important feature of the direction preference map. Continuity in the orientation map, however, seems to take precedence over continuity in the direction map. In principle, continuity in both maps could be equally preserved if there were 360°, not 180° pinwheels where each orientation appeared twice[15,16], but such 360° pinwheels have not been observed in the visual cortex of any species[4,7,12,13,17].

In conclusion, we have demonstrated that direction preference, like orientation preference, is systematically mapped in primary visual cortex. Our results are consistent with the evidence from closely spaced microelectrode recordings suggesting an ordered

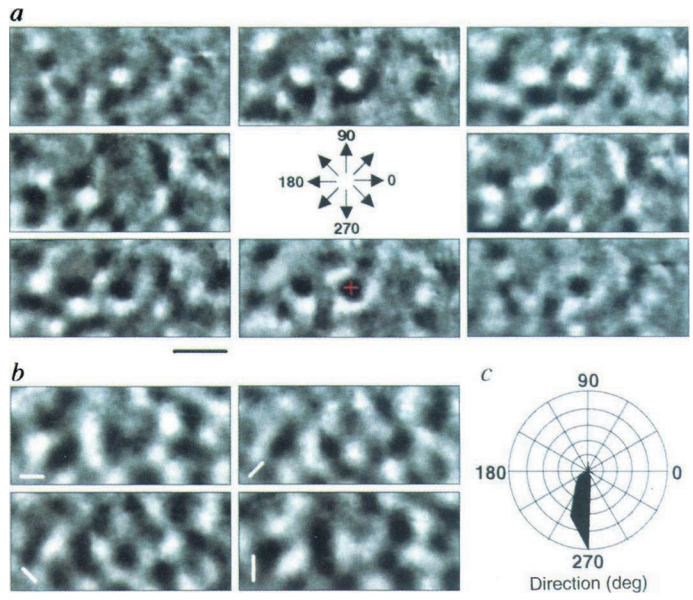


FIG. 1 Optical imaging of iso-direction and iso-orientation domains in area 17 of ferret visual cortex. *a*, Differential images of iso-direction domains produced by subtracting images obtained from oppositely moving stimuli. The horizontal arrow pointing to the right corresponds to 0°, whereas 90° is up. The dark regions were strongly activated by movement in the direction indicated by the arrows; light regions were strongly activated by movement in the opposite direction. Iso-direction domains typically appeared as circular or elongated regions of cortical activation, where domains having opposite direction preference were often paired. Scale bar, 1 mm; applies to *a* and *b*. *b*, Differential images of iso-orientation domains. The animal viewed the same stimuli used in *a* but moving in both directions during each presentation. These maps were produced by subtracting images obtained from orthogonal stimuli. Dark regions were strongly activated by the orientation shown in the lower left corner of each panel. In general, orientation domains had a more banded or striped appearance, and were typically larger in size and more uniform in their distribution than direction domains. *c*, Normalized polar diagram showing response versus stimulus direction for a group of neurons recorded at the site marked by the red cross in the lower middle panel in *a*. The neurons were strongly selective for a horizontal elongated bar moving downward (270°), and were located within the centre of an isodirection domain.

METHODS. Experiments were conducted using 13 animals with similar results. Optical imaging was performed as previously described[12,13]. Images were acquired using an enhanced video acquisition system (Optical Imaging Inc.). Ferrets (postnatal day 43–60) were anaesthetized with a mixture of ketamine hydrochloride (40 mg per kg intramuscularly (i.m.) and xylazine hydrochloride (2 mg per kg i.m.). A hole (6 mm × 12 mm) was made in the cranium over area 17, the dura was removed, and a stainless steel chamber was mounted to the skull, filled with saline, and sealed with a coverglass. Ferrets were paralysed with pancuronium bromide (2–4 mg $kg^{-1}$ interperitoneally) to prevent eye movements and artificially respirated with a mixture of 2:1 $N_2O$:$O_2$ supplemented with 0.5–1.0% halothane. Expired $CO_2$ was maintained at 4–5%. Visual stimulation was provided monocularly through the contralateral eye. The stimulus consisted of an array of randomly placed high-contrast bars (1.2° × 4.2°) that was drifted by 12–20 deg $s^{-1}$. The average density of bars was 2.5 bars per 10° × 10° region. The orientation of the bars always remained perpendicular to the direction of motion. The stimulus was shown first for 1 s before each period of recording video images. Images were then acquired for 3–15 s during continued stimulus presentation. Direction and orientation preference maps were acquired during separate interleaved sessions. In direction preference mapping sessions, the stimulus was moved in one direction throughout each acquisition period. Stimuli were paired so that an acquisition period with the stimulus moving in one direction was followed by an 8-s interstimulus interval (screen blank) and then another acquisition period during which the stimulus moved in the opposite direction. Multiple direction mapping sessions for each of four pairs of directions were conducted. In orientation selectivity mapping sessions the stimulus was drifted back and forth during each acquisition period, and stimuli were paired so that an acquisition period with the stimulus at one orientation was followed by an 8-s interstimulus interval and then an acquisition period with the stimulus at the orthogonal orientation. Multiple orientation mapping sessions for each of two pairs of orientations were conducted. In direction and orientation mapping sessions, 15–30 stimulus pairs were presented and all data acquired for each orientation and direction were averaged. We confirmed that this method of paired stimulus presentation produced the same results as when both orientation and direction maps were derived from a single set of acquired images (a single experiment with random presentation of 8 single-direction stimuli). Stimulus pairing, however, consistently produced images with a better signal-to-noise ratio. Images were acquired at a resolution of 655 by 480 pixels which corresponds to 13 μm per pixel with our camera optics. All differential images were smoothed with kernels ranging from 5–13 pixels, to reduce noise.

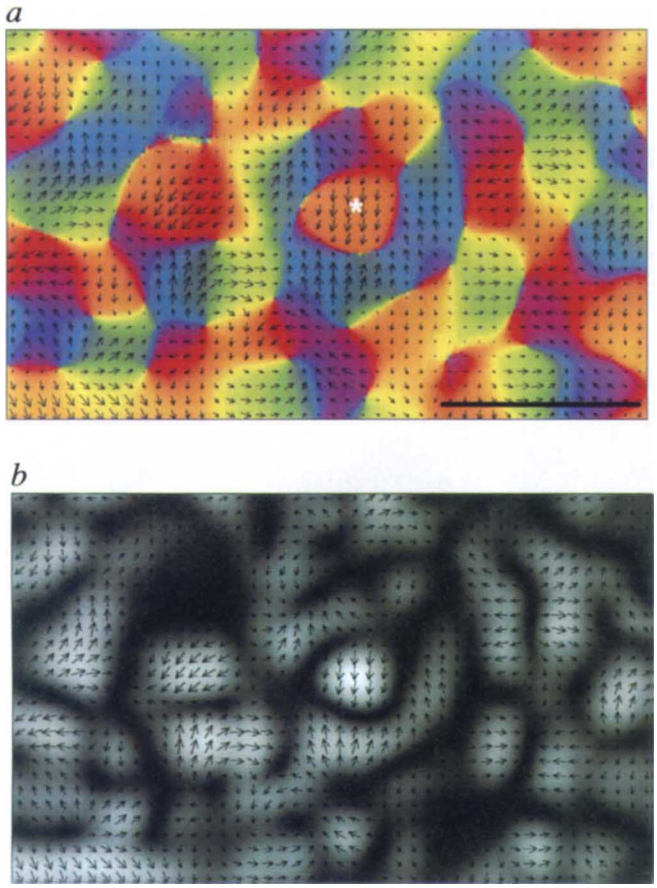


FIG. 2 Map of direction preference, produced by vectorially summing the images shown in Fig. 1*a*. *a*, The direction of best response is colour coded and represented by arrows overlaid on the map. The length of the arrow indicates the magnitude of the direction signal; long arrows represent regions highly selective for direction of motion, short arrows represent regions that were relatively unselective. The map consists of numerous regions with high selectivity in which direction preference smoothly changes. These regions are separated by regions of low selectivity across which direction preference abruptly changes, often by 180°. The white asterisk marks the location of the recording site whose directional response is shown in Fig. 1*c*. The preferred direction of the site (270°, downward vertical motion) matches the directional preference of the region of the map in which it was located (downward vertical arrows). Scale bar, 1 mm. *b*, Magnitude of direction signal for the map shown in *a*. Distribution of direction preference is shown superimposed on a map where light areas represent regions with high directional selectivity and dark regions represent regions with low selectivity. The map is broken up by numerous bands, or lines of low selectivity. These bands coincide with regions of the map where direction preference also changes most rapidly (see Fig. 3).

METHODS. Maps of direction preference were produced by vectorially summing the 8 differential images (as shown in Fig. 1*a*) on a pixel by pixel basis according to previously described methods[4,7]. Arrow lengths are linearly scaled to the magnitude of the resulting vector.

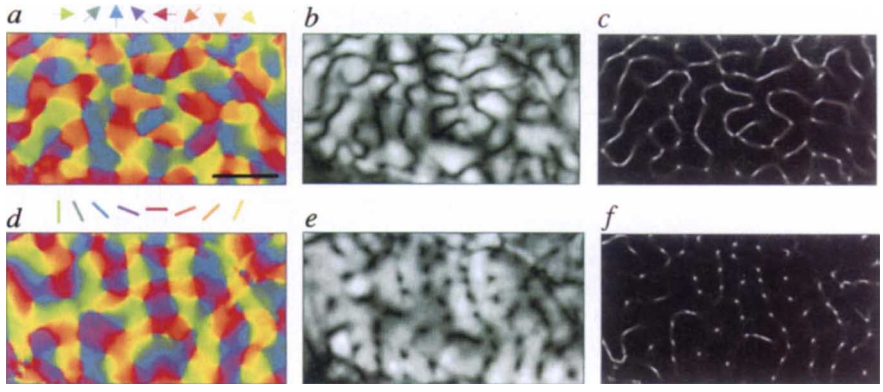


FIG. 3 Comparison of direction and orientation preference maps. Direction maps are shown in *a*–*c* whereas orientation maps obtained from the same cortical region are shown in *d*–*f*. Angle maps are shown in the first column (*a*, *d*); direction and orientation preference are colour coded according to the key above each map. Magnitude maps are shown in the middle column (*b*, *e*); black indicates low selectivity. Rate of change maps are shown in the last column; white indicates high rate of change. Although both orientation and direction are continuous locally and discontinuous globally, they differ significantly in the spatial organization of the discontinuities. The direction map is broken up into patches and strips by numerous lines of low selectivity (*b*) and high rate of change (*c*). In contrast, the orientation map is dominated by singularities: more punctate regions of low selectivity (*e*) and high rate of change (*f*) that correspond to the centres of pinwheels. Scale bar (in *a*), 1 mm; applies to *a*–*f*.

METHODS. Angle, magnitude, and rate of change maps were calculated according to previously described methods[4,7]. In the magnitude maps, a cortical site with a small response magnitude may reflect one of two conditions: 1) all or many orientations or directions evoke a strong response, or 2) one or very few nearby orientations or directions evoke a weak response. Although these two conditions cannot be distinguished, they both represent a cortical site with low selectivity to the particular stimuli within the resolution limits of our methods.

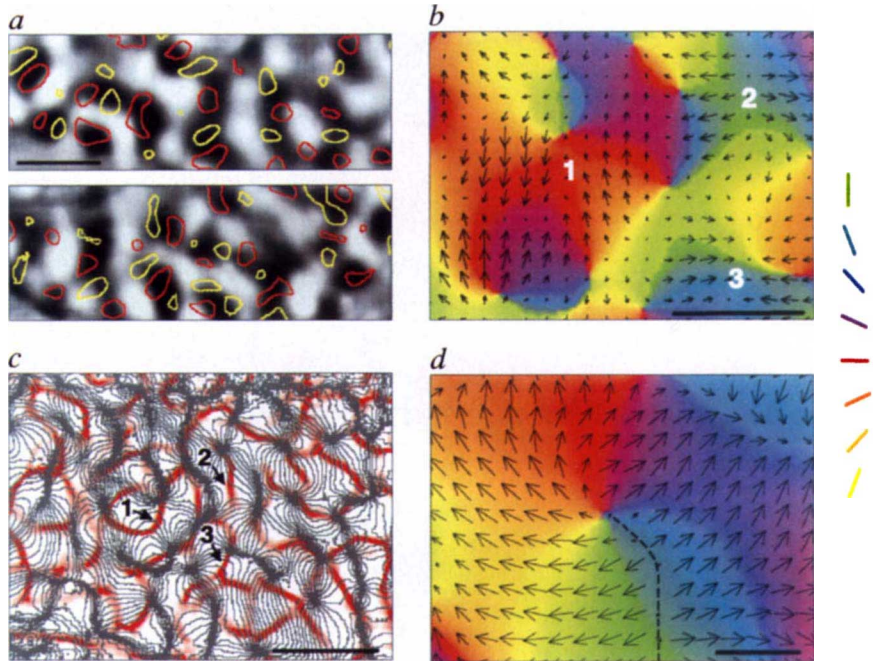


FIG. 4 Relationship between direction and orientation preference maps. *a*, Iso-direction domains for horizontal motion, 0° (red) and 180° (yellow), are shown superimposed on iso-orientation domains obtained using the same stimulus angle (vertical bars) for two animals. Iso-orientation domains activated by these stimuli appear dark in the image. Domains that prefer opposite directions of motion lie adjacent to each other and conform to the shape of the iso-orientation domains. Scale bar, 1 mm. *b*, Iso-orientation regions are subdivided into patches with opposite direction preference. Direction preference map (arrows) is superimposed on an orientation preference map (colours). Orientation preference is colour coded according to the legend shown to the right of the image. 1 is located at the centre of a region of the orientation map preferring horizontal bars (red). To the left and right of 1 are two direction patches with opposite preferred directions of motion (up/down). 2 and 3 mark orientation regions preferring vertical bars (green/blue) which are subdivided into patches preferring left/right directions of motion. These directions are orthogonal to the corresponding orientation preference. The preferred direction of motion was orthogonal, or within 45° of orthogonal, to the preferred orientation in 73.2 ± 2% of pixels ($n = 5$ animals). Sites with very weak directional selectivity (magnitude of directional response below 20% of maximum) were excluded from this calculation. This relationship is to be expected as stimulus motion was always along an axis orthogonal to its orientation. Scale bar, 500 μm. *c*, Relationship between fractures in the direction preference map (red) and iso-orientation contours (grey). This image is a lower magnification view of the cortical region shown in *b* including surrounding areas. The numbers point to the corresponding sites labelled in *b*. Direction fractures bisect regions where orientation preference shifts in a gradual fashion. Although at the numbered sites, as well as other locations in the map, direction fractures intersect orientation contours at right angles, a statistically significant bias towards orthogonality was not found. The fractures also frequently intersect orientation pinwheel centres, which are seen as dark zones from which contour lines radiate. In some cases, multiple fractures radiate from a single pinwheel centre. Scale bar, 1 mm. *d*, Organization of direction preference around an orientation pinwheel. Direction preference arrows are superimposed on a colour-coded map of orientation (colour case as *b*). Direction preference shifts continuously with orientation around the pinwheel except at the fracture (dashed line) where contiguous cortical regions have opposite direction preferences. Scale bar, 200 μm.

arrangement of direction selective responses in area 17 and 18 of the cat visual cortex[8–10] and with the descriptions of orientation and direction preference maps in cortical area MT of the owl monkey[14]. Thus, orderly maps of direction and orientation preference seem to be a general feature of primary, as well as more specialized, visual cortical areas. □

Received 8 September; accepted 13 December 1995.

1. Hubel, D. & Wiesel, T. N. *J. Physiol., Lond.* **195,** 215–243 (1968).
2. Hubel, D. & Wiesel, T. N. *J. comp. Neurol.* **158,** 267–294 (1974).
3. Hubel, D. & Wiesel, T. N. *Proc. R. Soc. Lond.* B **198,** 1–59 (1977).
4. Blasdel, G. G. & Salama, G. *Nature* **321,** 579–585 (1986).
5. Blasdel, G. G. *J. Neurosci.* **12,** 3115–3138 (1992).
6. Bonhoeffer, T. & Grinvald, A. *Nature* **353,** 429–431 (1991).
7. Bonhoeffer, R. & Grinvald, A. *J. Neurosci.* **13,** 4157–4180 (1993).
8. Payne, B. R., Berman, N. & Murphy, E. H. *Brain Res.* **211,** 445–450 (1981).
9. Tolhurst, D. J., Dean, A. F. & Thompson, I. D. *Expl Brain Res.* **44,** 340–342 (1981).
10. Swindale, N. V., Matsubara, J. A. & Cynader, M. S. *J. Neurosci.* **7,** 1414–1427 (1987).
11. Frostig, R. D., Lieke, E. E., Ts'o, D. Y. & Grinvald, A. *Proc. natn. Acad. Sci. U.S.A.* **87,** 6082–6086 (1990).
12. Weliky, M. & Katz, L. C. *J. Neurosci.* **14,** 7291–7305 (1994).
13. Weliky, M., Kandler, K., Fitzpatrick, D. & Katz, L. C. *Neuron* **15,** 541–552 (1995).
14. Malonek, D., Tootell, R. B. H. & Grinvald, A. *Proc. R. Soc. Lond.* B **258,** 109–119 (1994).
15. Swindale, N. V. *Proc. R. Soc. Lond.* B **215,** 211–230 (1982).
16. Braitenberg, V. & Braitenberg, C. *Biol. Cybern.* **33,** 179–186 (1979).
17. Fitzpatrick, D., Schofield, B. R. & Strote, J. *Soc. Neurosci. Abstr.* **20,** 837 (1994).

ACKNOWLEDGEMENTS. We thank N. Cant, K. Kandler and D. Purves for helpful comments on the manuscript. We thank L. C. Katz for support (M.W.). This work was supported by NIH grants to D.F. and L.C. Katz.

# Long-range synchronization of oscillatory light responses in the cat retina and lateral geniculate nucleus

**Sergio Neuenschwander & Wolf Singer***

Max-Planck-Institut für Hirnforschung, Deutschordenstrasse 46, 60528-Frankfurt a.M., Germany

**VISUAL responses in the retina and the lateral geniculate nucleus (LGN) exhibit oscillatory patterning within a broad range of frequencies[1–9]. Oscillatory activity is often associated with the synchronization of spatially distributed responses[10]. Here we demonstrate, with simultaneous multi-electrode recordings from the retina and the LGN, that stationary and moving light stimuli evoke in retinal ganglion cells oscillatory responses in the frequency range of 61 to 114 Hz that become synchronized over distances larger than 20 degrees of visual angle across the nasal and temporal halves of the retina. This temporal patterning of retinal responses is transmitted reliably by LGN neurons, such that stimuli crossing the vertical meridian evoke synchronous responses in the LGNs of both hemispheres. The oscillatory responses are not phase-locked to the stimulus onset, indicating that synchronization results from horizontal interactions in the retina. The occurrence of synchronization depends on global stimulus properties such as size and continuity, suggesting that temporal correlation among responses of spatially segregated ganglion cells can be exploited to convey information relevant for perceptual grouping.**

Simultaneous recordings from a total of 153 pairs of recording sites were obtained with up to four independently driven microelectrodes from neurons located either within the same LGN or in the LGNs of the two hemispheres in 17 anaesthetized cats. The receptive fields of the neurons were typically non-overlapping and, depending on the combination of recorded laminae, cells at

* To whom correspondence should be addressed.